

# Handling of large and heavy objects using a single mobile manipulator in combination with a roller board<sup>☆</sup>

Tobias Recker<sup>\*</sup>, Florian Heilemann, Annika Raatz

Leibniz Universität Hannover, Institute of Assembly Technology, An der Universität, Garbsen 30823, Germany

## ARTICLE INFO

### Article history:

Received 20 September 2019

Revised 19 March 2020

Accepted 25 May 2020

### Keywords:

Tractor-trailer wheeled robot

Null space motion

Object handling

## ABSTRACT

This paper presents a method for autonomous loading, transportation, and unloading of large objects using a nonholonomic mobile manipulator. Here, the size of the transported object is considerably larger than the size of the mobile platform, which is made possible through the use of a roller board. In this way, the mobile manipulator can handle objects that exceed the manipulator's payload. The robot can load and unload the object onto its platform using the differential kinematics of the system for a null space motion to maintain the object's position in space. In order to localise the object, we apply 3D-perception using a depth-camera. While transporting the object to its destination, the robot is considered a tractor-trailer-wheeled system and can navigate using SLAM. Kinematic modelling and practical evaluation prove that the system can potentially take over arduous transportation tasks.

© 2020 Gottfried Wilhelm Leibniz Universität Hannover. Published by Elsevier B.V. This is an open access article under the CC BY-NC-ND license (<http://creativecommons.org/licenses/by-nc-nd/4.0/>)

## 1. Introduction

Large and heavy robots are often needed to transport large or heavy components. These robots not only cost more than smaller robots, but they also consume more power and occupy additional hall space. As flexible and intelligent robotics in assembly become more important Krüger et al., it becomes necessary to consider how to increase the capabilities of smaller robots.

In this work, we deal with the transport of heavy objects (compared to the payload) using a passive auxiliary device. As an example of a passive auxiliary device, we use a conventional roller board. An aluminum construction profile that exceeds the maximum payload of our robot by 60 % serves as the payload. To enable transportation, one end of the profile is supported on a roller board (see Fig. 1). In this way, the effective payload of our robot can be doubled when transporting long objects. The resulting system consists of a mobile manipulator which, similar to a tractor-trailer-wheeled robot, pulls the passive roller board behind it as a trailer. With this, the transport object forms the connection between the tractor and the trailer. For our tests, we use a nonholonomic robot, as nonholonomic robots are less dependent on the flatness and quality of the floor and thus offer a wider range of



Fig. 1. Mobile Universal Robot (MuR) 205 carrying a construction profile.

applications. Possible applications include automating construction sites or processes or in intralogistics as our method does not require a structured environment.

After presenting the basic concept in Section 1.2, we will give a short overview of related work. Since our mobile manipulator is redundant and nonholonomic with 8 (6 + 2) degrees of freedom, we will subsequently deal with kinematic modelling. After the description of the hardware and the experimental setup, we will validate our approach with two series of measurements.

### 1.1. Related work

In the past, there have already been many attempts to realise cooperative object transport using a group of nonholonomic mobile robots (Tuci et al., 2018). Most work focuses on the transport of large objects with several small units. Here, the individual units

<sup>☆</sup> Peer review under the responsibility of the scientific committee of CIRP.

<sup>\*</sup> Corresponding author.

E-mail address: [Recker@match.uni-hannover.de](mailto:Recker@match.uni-hannover.de) (A. Raatz).

are still actively powered (Decentralized, 1996; Loh and Trachtler, 2012). While this serves to increase the capabilities and the payload of the resulting system, each of these robots needs its own control and power supply. Also, a more complex master control is often needed. This can significantly increase the cost of the overall system. Although there have been attempts to use passively moving auxiliary devices, these nevertheless usually require some form of actuation and communication (Ohashi et al., 2016).

Tractor-trailer-wheeled robots (TTWR) avoid this problem by towing a passive trailer through the active towing vehicle, similar to a truck. In this way the movements of the trailer depend exclusively on the movements of the tractor. By distributing the load between the robot and trailer, both larger and heavier objects can be handled. Kinematic modelling for such systems has already been presented by Khalaji et al. (2013) and Nakamura et al. (2000). The same applies to path planning (Svestka and Vleugels, 1995), which is simplified in our scenario by measuring the angle between the tractor and the trailer (see Section 1.2). In a TTWR, the trailer is usually coupled to the tractor through a rigid metal rod, which is part of the trailer (Kassaeiyan et al., 2019; Khalaji et al., 2013). However, according to the authors' knowledge, the use of the work piece as a link between the tractor and trailer has not yet been investigated. By using the handling object as a link, we achieve a flexible system with regard to the workpiece size, given the object is able to withstand the forces occurring during transport. Also, there are advantages in terms of autonomous loading, as the mobile manipulator can move independently from the trailer.

### 1.2. Basic concept

At the beginning of the transport process, the construction profile is located on the floor. Using image processing, we detect the position of the profile and subsequently determine the position of the ends. The mobile robot then moves to the first end of the profile and places the roller board next to it. The roller board is carried by the robot and placed in the correct position before placing the first end on top of it. Afterwards, the mobile base moves to the other end of the profile. The manipulator grasps the profile and raises it vertically to the height of its loading platform. As one end of the profile is always supported on the floor or the roller board, the manipulator only has to lift half the profile's weight.

After the second end of the profile has reached the desired height, the robot performs a null space motion (NSM). The NSM is used to move the mobile base under the second end of the profile while not moving the profile. This turned out to be necessary after we found that the conventional loading of the profile, by moving the end effector when the base is stationary, often resulted in the profile slipping on the roller board or inside the gripper. Since the position of the profile's end cannot be measured (currently), we try to minimise the displacement.

The entire loading process, starting with the initial grasping of the profile, is shown in Fig. 2. Due to the mobile base being non-holonomic, it is not possible for the base to move directly in the y-direction to get under the end of the profile. Instead, we move the robot in the trajectory shown in Fig. 3 to move the base below the end of the profile. In this case, it is not possible to turn the mobile platform in the direction of the target point and then drive straight to the target position, as the arm structure would collide with itself.

After the profile has been loaded, as shown in Fig. 2, it is transported to the destination. We use a conventional path planner (SBPL-lattice) to create a global path. For our local path planner, we adapt the existing local path at corners and obstacles so that there is no collision of the profile with the surroundings. For this,

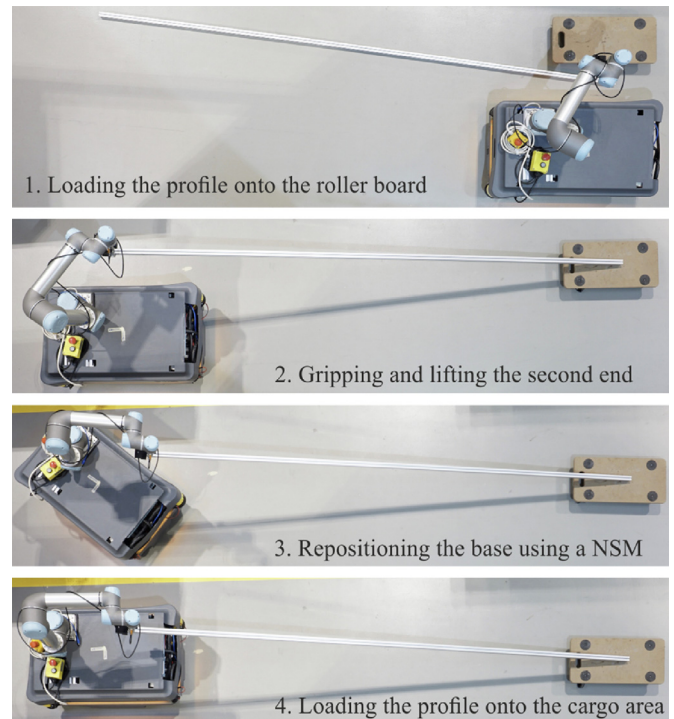


Fig. 2. Loading an aluminum profile onto the MuR205.

we dynamically calculate the outer contour of the base, profile, and roller board. The outer contour of the overall system depends essentially on the length of the profile and the position of the roller board, as shown in Fig. 4.

With known position  $\vec{P}_1$  and angle  $\alpha$  the position of the roller board results in:

$$\vec{P}_3 = \begin{bmatrix} P_{1,x} - l_1 \cdot \cos(\vartheta) - l_2 \cdot \cos(\alpha - \vartheta) \\ P_{1,y} - l_1 \cdot \sin(\vartheta) + l_2 \cdot \sin(\alpha - \vartheta) \end{bmatrix} \quad (1)$$

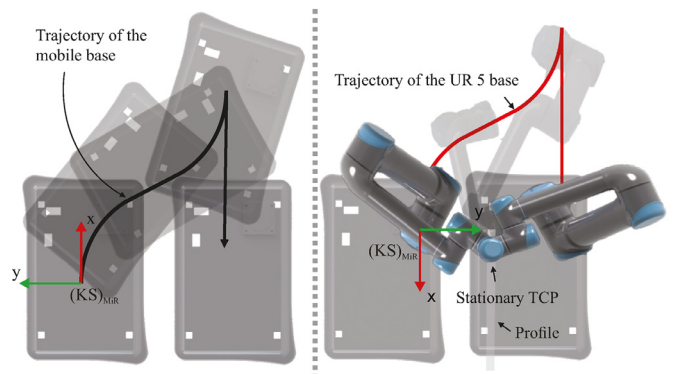


Fig. 3. Movement of the mobile base and UR 5 while loading a workpiece.

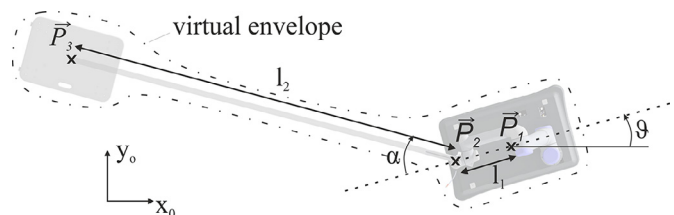


Fig. 4. Top view of the MuR 205 & roller board carrying a construction profile.

The length of the profile is constant during transport and can either be taken from the CAD data or determined using image processing. To determine the angle  $\alpha$  we use the encoders of the manipulator. In the transport position, the sixth axis of the manipulator is set perpendicular to the profile. The angle of the profile to the platform (the ground)  $\beta$  is determined by the difference between the height of the mobile platform  $z_m$  and the roller board  $z_r$  and the length of the profile  $l_2$  (Eq. (2)).

$$\beta = \arccos\left(\frac{z_m - z_r}{l_2}\right) \quad (2)$$

If the last robot axis is set to use impedance-control, no torque is applied to the profile, which allows free rotation of the profile around the center of rotation  $\vec{P}_3$ . The drive position of the sixth axis  $q_6$  then corresponds to the angle  $\alpha$ . This significantly reduces the effort required to determine the footprint while increasing the accuracy, since  $\alpha$  does not have to be estimated by an observer. To place the profile, the picking process is inverted, whereby it is important to ensure that the roller board does not obscure the placement position at the end of the transport.

In the context of this article, we would like to focus in particular on the process of loading and the accuracy in determining the envelope for collision avoidance.

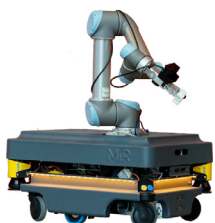
## 2. Setup

In this chapter, we will introduce our mobile manipulator, the MuR 205 in detail and explain the measurement setup and the work piece.

### 2.1. Hardware setup

The Mobile Universal Robot 205 (MuR 205) consists of a non-holonomic robot platform (MiR200) and a 6-axis industrial robot (UR5). The MiR 200 is equipped with two Sick laser scanners, odometry, ultrasonic sensors and a 3D camera. Another 3D camera (Intel Realsense D435) is attached to the gripper of the UR5. In order to counteract the tilting of the robot when handling loads, an attempt was made to keep the center of mass of the robot as low as possible. We integrated the UR5's controls into the MiR's case and replaced the lightweight lithium batteries with heavier lead batteries. Due to this change, there is no risk of tipping over, even at full speed. We integrated a x86 based control PC running the Robot Operating System (ROS) to control our robot. An overview of the performance data can be found in table 1. We use custom gripper jaws for the RG2 gripper which have been designed to fit into the notch of the profile, ensuring a form-fit connection. The roller board is a typical commercial model with four wheels able to carry around 200 kg. The two rear rollers were fixed so that the roller board is always oriented in the direction of motion.

**Table 1**  
MuR 205 Performance Data.

MuR 205	Specification	Property
	Length	890 mm
	Width	580 mm
	Weight	99.0 kg
	Payload	5 kg
	Speed	2.2 m/s
	Battery capacity	1590 Wh (8h)
Reach	850 mm	
Number of axes	8	

### 2.2. Handling object

The test object is a square (40 mm x 40 mm) aluminium construction profile with a length of 3 m. The weight of a single profile is 4 kg which is within the specified payload, therefore two profiles are connected. In combination with the weight of the gripper (740 g), the maximum payload of the manipulator is exceeded by 75 %. Due to the length of 3 meters, the profile is also considerably too large to be placed entirely on the platform.

### 2.3. Experimental setup

To measure the position of the robot in space, we use a calibrated laser tracker (Faro Vantage S6) with an accuracy of  $16 \mu m$ . The target for our tracker is attached to the end effector of the robot beside the camera. At a distance of 5 m and a measuring frequency of 250 Hz, we can achieve a total accuracy of  $20 \mu m$  for the position.

To validate the two main aspects “loading process” and “envelope determination” focused in this article, we created two measurement scenarios. In the scenario “loading process”, we move the mobile basis as shown in Fig. 3. Moving along the given trajectory, the base travels a distance of about 2.3 m. At the end of the movement, the position in x-direction is identical to the start position, while in y-direction it is offset by 407 mm. Meanwhile, we measure the displacement of the profile using the laser tracker. Due to the measuring principle of the tracker, we can only measure the 3-DOF position accuracy but not the angular errors.

In the second scenario, “envelope determination”, we examine the accuracy of the determination of the roller board position. We move the roller board by hand while the MuR 205 is stationary. Moving the roller board causes the profile to rotate which changes  $\alpha$ . Meanwhile we record the position of the roller board using our laser tracker. We then compare the position calculated by using  $q_6$  as  $\alpha$  (see Eq. (1)) with the position measured by the tracker. Comparing the calculated with the measured position shows how accurately the envelope of our TTWR can be determined during the movement of the MuR 205.

In order to conduct any measurement regarding the NSM, we will first need to resolve the redundancy of our MuR 205. For this we will describe the kinematics of our robot in the next section and set up constraints to handle the two redundant degrees of freedom.

## 3. Kinematic modelling and control

In this section, we formally describe the kinematics of our system to control the manipulator and mobile base as one robot. Considering the system as a single unit enables the use of the inherent redundant degrees of freedom specifically for simultaneous motions of the arm and mobile base. This allows us to fully exploit the advantages of adding more joints to the kinematic chain. For the loading process, the robot performs a NSM. So while the mobile platform is moving, the end effector will stay stationary. To achieve this behaviour, a complete kinematic model of the robot is needed, in order to control the robot. As the modelling of nonholonomic mobile manipulators is extensively described in Gardner and Velinsky (2000) and Bayle et al. (2003) we will not go into detail here.

To model the forward kinematics of the system, different coordinate systems for the individual components are required (see Fig. 5). The coordinate system  $(KS)_{World}$  serves as the global reference frame, where all tasks are defined. The topologically following coordinate system  $(KS)_{MiR}$  is used for the mobile platform and its differential drive modelling. The respective transformation between those can be obtained by computing the Odometry or using



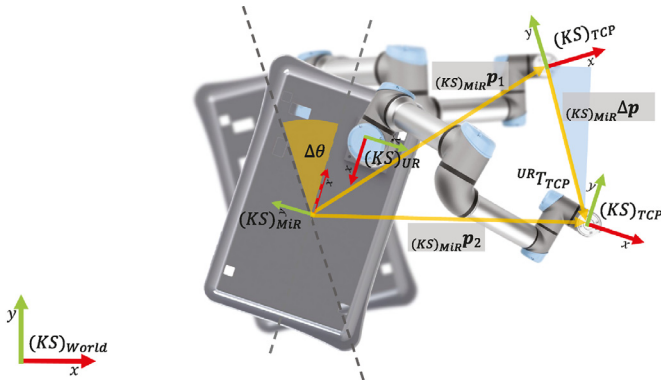


Fig. 5. Coordinate systems and resulting end effector velocities  $\Delta\vec{p}$  when rotating the mobile base about  $\Delta\theta$  with static manipulator configuration.

Simultaneous Localization and Mapping (SLAM). The rigid-body-transformation between  $(KS)_{MiR}$  and  $(KS)_{UR}$  was calibrated using the previously mentioned laser tracker. The last transformation between  $(KS)_{UR}$  and  $(KS)_{TCP}$  can be computed by using the forward kinematics of the manipulator. This results in the full kinematic chain of the mobile manipulator MUR 205 and can be written as in Eq. (3).

$$\text{World}\mathbf{T}_{TCP} = \text{World}\mathbf{T}_{MiR} \cdot {}^{MiR}\mathbf{T}_{UR} \cdot {}^{UR}\mathbf{T}_{TCP} \quad (3)$$

The forward kinematics are a closed-form solution and can always be solved explicitly so that the position of the end effector in respect to the global reference frame  $(KS)_{World}$  is known at any time. Furthermore, it is desirable to compute the differential kinematics, especially when using velocity-based position controllers, as we are throughout this application. The velocities of the end effector in dependence of the joint velocities are computed using the Jacobian  $\mathbf{J}_{MuR}^{6 \times 8}$  of the whole robot:

$$\begin{bmatrix} \dot{x} \\ \dot{y} \\ \dot{z} \\ \dot{\alpha} \\ \dot{\beta} \\ \dot{\theta} \end{bmatrix} = \mathbf{J}_{MuR}^{6 \times 8} \cdot \begin{bmatrix} \dot{q}_1 \\ \dot{q}_2 \\ \dot{q}_3 \\ \dot{q}_4 \\ \dot{q}_5 \\ \dot{q}_6 \\ \dot{q}_l \\ \dot{q}_r \end{bmatrix} \quad (4)$$

When setting up the Jacobian  $\mathbf{J}_{MuR}^{6 \times 8}$ , the additional wheel velocities  $\dot{q}_l$  and  $\dot{q}_r$  can be attached to the joint velocity vector of the manipulator. This results in a non-quadratic Jacobian matrix, which means there are infinite solutions for the inverse differential kinematics. This is due to the redundancy in the system.  $\mathbf{J}_{MuR}^{6 \times 8}$  can be composed of modified Jacobians of the individual subsystems mobile base and manipulator as shown in Eq. (5).

$$\mathbf{J}_{MuR}^{6 \times 8} = [\mathbf{J}_{UR}^{6 \times 6} \quad | \quad \tilde{\mathbf{J}}_{MiR}^{6 \times 2}] \quad (5)$$

The modified Jacobian of the mobile platform  $\tilde{\mathbf{J}}_{MiR}^{6 \times 2}$  factors the resulting velocities of the end effector that are induced from pure velocities of the mobile platform. Therefore, the regular Jacobian of the mobile platform is multiplied with the skew-matrix in the center of Eq. (6), which takes into account the cross-product of angular velocities of the mobile platform and the current lever arm of the manipulator. The lever arm of the manipulator in respect to the mobile base's center is noted with  $p_i$ . The formalism in Eq. (6) transforms angular velocities of the mobile platform to cartesian velocities of the end effector, with given radius of the

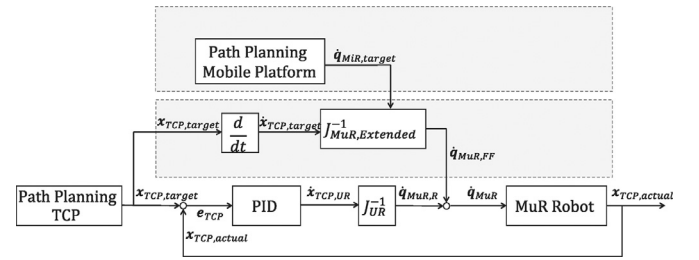


Fig. 6. Feed-forward PID-Controller for redundancy resolution.

wheels  $r$  and wheel distance  $d$ .

$$\tilde{\mathbf{J}}_{MiR}^{6 \times 2} = \begin{bmatrix} \text{World}\mathbf{R}_{MiR} & \mathbf{0} \\ \mathbf{0} & \tilde{\mathbf{J}}^{3 \times 3} \end{bmatrix} \cdot \begin{bmatrix} 1 & 0 & 0 & 0 & p_z & -p_y \\ 0 & 1 & 0 & -p_z & 0 & p_x \\ 0 & 0 & 1 & p_y & -p_x & 0 \\ 0 & 0 & 0 & 1 & 0 & 0 \\ 0 & 0 & 0 & 0 & 1 & 0 \\ 0 & 0 & 0 & 0 & 0 & 1 \end{bmatrix} \cdot \begin{bmatrix} \cos\theta \cdot \frac{r}{2} & \cos\theta \cdot \frac{r}{2} \\ \sin\theta \cdot \frac{r}{2} & \sin\theta \cdot \frac{r}{2} \\ 0 & 0 \\ 0 & 0 \\ 0 & 0 \\ -\frac{r}{2d} & \frac{r}{2d} \end{bmatrix} \quad (6)$$

Computing Eq. (4) yields the closed-form solution for the differential kinematics. To fully control the robot during the NSM, the inverse solution of the differential kinematics is required. Due to the system's redundancy, the inverse kinematics also has infinite solutions. To solve the redundancy, additional conditions have to be added to the kinematic system. Besides the well known Moore-Penrose pseudoinverse, the Extended-Jacobian method was used, to explicitly define the kinematic problem (De Luca et al., 2006). Eq. (7) shows the attached sub-condition  $\mathbf{H}^{2 \times 8}$ , so that the system results in a quadratic form and is therefore invertible.

$$\begin{bmatrix} \dot{x} \\ \dot{y} \\ \dot{z} \\ \dot{\alpha} \\ \dot{\beta} \\ \dot{\theta} \\ y_1 \\ y_2 \end{bmatrix} = \begin{bmatrix} \mathbf{J}_{MuR}^{6 \times 8} \\ \mathbf{H}^{2 \times 8} \end{bmatrix} \cdot \begin{bmatrix} \dot{q}_1 \\ \dot{q}_2 \\ \dot{q}_3 \\ \dot{q}_4 \\ \dot{q}_5 \\ \dot{q}_6 \\ \dot{q}_l \\ \dot{q}_r \end{bmatrix} \quad (7)$$

Using the previously explained methods the feed-forward controller displayed in Fig. 6 performs NSMs, that obey the redundancy resolution criteria. The controller is split into three components. The basic loop is a velocity-based position controller that holds the desired target position and uses the arm to correct position errors, that is induced by external disturbances. The feed-forward loop combines the motion planning for the TCP and the mobile base. It predicts the desired joint speeds using inverse differential kinematics to accomplish the desired end effector velocity. The wheel velocities for the mobile base serve as constraints for the redundancy resolution. The feed-forward controller is mainly used to reduce the following error during motions since it incorporates all given kinematic information.

#### 4. Experimental results

In the first experiment, we compare the loading process without NSM to that with NSM. We use the feed-forward PID controller

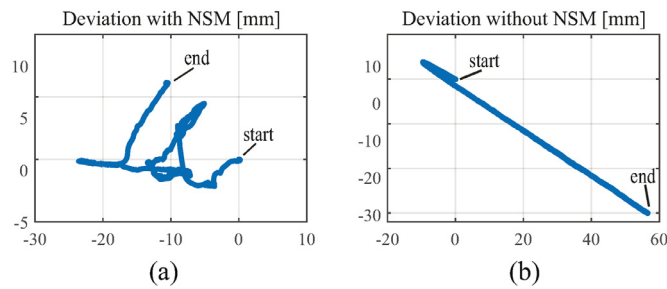


Fig. 7. Movement of the profile on the roller board during loading using NSM (a) and without NSM (b).

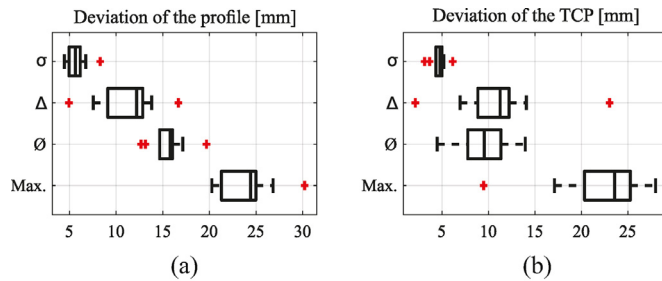


Fig. 8. Deviation of the profile (a) and TCP (b) during loading.

presented in Section 3 to control the manipulator during the NSM. The parameters of our controller were set empirically. Since the controller determines the position error using the odometry of the mobile base and the direct kinematics of the manipulator, we first measured the average slip for our trajectory. In a series of tests, we measured an average error caused by the slip of about 5.7 mm. As the odometry does not register the slip of the wheels, all subsequent measurements contain an error of about 5.7 mm due to the drift of the platform. In general, it would be possible to compensate for the drift of the platform using advanced Monte Carlo localization (AMCL) as our robot is equipped with laser scanners. However, we found the error in our trajectory was too low to be efficiently compensated by AMCL. Fig. 7 shows the movements of the end of the profile placed on the roller board during an exemplary loading process. The starting position was set to (0|0). For our measurements, we only consider the x-y plane, as the movement of the mobile base only takes place in this plane. To enable a meaningful comparison, we use the best possible starting position for the measurement without NSM. The end of the profile is located exactly to the side of the robot so that it only has to be moved in y-direction. A different starting point would cause an additional error in the x-direction.

In the measurement shown in Fig. 7, we measured a maximum deviation of 23.56 mm for the NSM (a) and 64.1 mm for the conventional loading process (b). This is despite the fact that we chose the optimal situation for the conventional loading process. On average the maximum displacement was 22.1 mm (see Fig. 8 (a)) for the NSM and 64.1 mm without the NSM. All measurements were repeated 15 times. In our tests, the standard deviation of the movement without NSM was only 0.2 mm, as it is solely determined by the repeatability of the manipulator. In general, the error with NSM is considerably smaller although in both cases, it is still very small compared to the dimensions of the roller board (290 mm x 590 mm).

Besides the deviation of the position, we would also like to consider the angular error. Since we can only measure one point at a time without angular information, as described above, we had to make an additional series of measurements for the TCP. By comparing the deviations of the TCP with the deviations of the profile

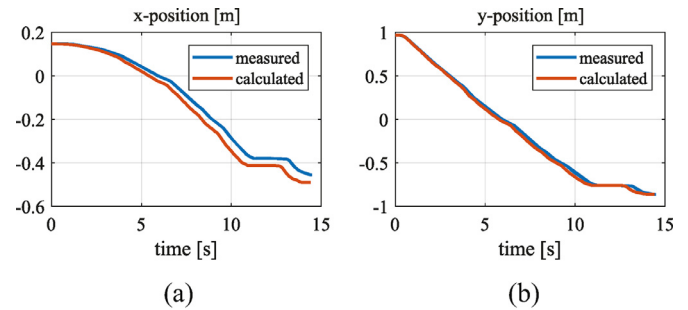


Fig. 9. Comparison of calculated position (a) against the measured position (b).

on the roller board, we try to get an impression of the resulting angular error. With the exception of the average error, the results in both measurements (compare Fig. 8 (a) and (b)) are very similar. From this, it can be concluded that the angular error of the TCP is either compensated by the elasticity of the gripper or is rather small.

In addition to the deviations during the movement, we also examined the difference  $\Delta$  between the start and end position. This difference was on average 11 mm (profile) and 11.4 mm (TCP) in our measurements. Of these, about 5.7 mm are caused by slip as described. The remaining deviations must, therefore, have a different origin. We attribute them mainly to small errors in the kinematic calibration of our manipulator. Also the difference in communication delays of our manipulator and the platform result in motion commands not being executed synchronously. This latency issue occurs since we are using ROS as an operating system which can not control the platform and the manipulator in real-time. In consideration of the small deviations during the loading and handling of the second end of the profile, we consider the assumption that the profile lies in the middle of the roller board to be justified.

Based on this assumption the second measurement scenario serves to determine if the position of the roller board relative to the robot can be estimated with sufficient accuracy. Fig. 9 (a) and (b) show a comparison of the position of the roller board measured with the laser tracker and the position calculated using Eq. (1). The position of the roller board is shown in the world coordinate system  $(KS)_{World}$ . The roller board is rotated along a circle around the base of the center of rotation  $\vec{P}_3$ . The radius of the circle equals the length of the profile (3 m). During the 1.95 m long movement, we measured a maximum error of 34.1 mm in x-direction and 33 mm in the y-direction. This translates into a deviation of 11 % relative to the size of the roller board. Considering the elasticity of the gripper and the profile, we consider this to be a very good approximation.

The results show that the position of the roller board and thus the envelope of our system can be determined very well during transport. Combined with the loading process described in Section 1.2, we can safely transport long and heavy objects with our MuR 205.

## 5. Conclusions and future work

In this paper we proposed an easy approach to double the effective payload of a mobile manipulator. After modelling the inverse kinematics we were able to use the redundancy of our mobile manipulator to perform a NSM with the robot. In this way, we could position a construction profile precisely on the robot's cargo area. The footprint of the resulting TTWR was calculated by measuring the encoder position of the hand axis of our manipulator. We carried out a series of tests to prove the functionality and efficiency of our approach. The experiments showed that by using an inverse model for feed-forward control we obtained very good re-

sults when performing a NSM. Also, we were able to validate the ability to transport almost any type of profile, even if the dimensions and weight exceed the capabilities of a single manipulator.

In future work we would like to extend our transport concept regarding the transport of various similar objects. By porting our code to a real-time capable version of ROS (ROS-Industrial) we hope to solve problems caused by communication delays and achieve even better accuracy in the future. Furthermore, the use of a NSM is also very interesting when using several robots with or without one or more roller boards. Since the manipulators do not change the position of the workpiece during loading, no additional force is applied to the workpiece.

### Declaration of Competing Interest

The authors declare that they have no known competing financial interests or personal relationships that could have appeared to influence the work reported in this paper.

### References

- Bayle, B., Renaud, M., Fourquet, J., 2003. Nonholonomic mobile manipulators: kinematics, velocities and redundancies. *J. Intell. Robot. Syst.* 36, 45–63.
- De Luca, A., Oriolo, G., Giordano, P. R., 2006. Kinematic modeling and redundancy resolution for nonholonomic mobile manipulators. In: *Proceedings ICRA 2006*, Orlando, FL, pp. 1867–1873.
- Decentralized, 1996. control of multiple robots handling an object. In: *Proceedings of IEEE/RSJ International Conference on Intelligent Robots and Systems. IROS '96*, Osaka, Japan, Vol. 1, pp. 318–323.
- Gardner, J.F., Velinsky, S.A., 2000. Kinematics of mobile manipulators and implications for design. *J. Robot. Syst.* 17, 309–320.
- Kassaeiyan, P., Tarvirdizadeh, B., Alipour, K., 2019. Control of tractor-trailer wheeled robots considering self-collision effect and actuator saturation limitations. *MSSP* 127, 388–411.
- Khalaji, A.K., Moosavian, S., Ali, A., 2013. Robust adaptive controller for a tractor-trailer mobile robot. In: *IEEE/ASME Transactions on Mechatronics*, Vol. 19, pp. 943–953. Nr. 3, S. 2013
- Krüger, J., Wang, L., Verl, A., Bauernhansl, T., Carpanzano, E., Makris, S., Fleischer, J., Reinhart, G., Franke, J., Pellegrinelli, S., Innovative control of assembly systems and lines. *CIRP Ann.* 66(2), 707–730.
- Loh, C.C., Trachtler, A., 2012. Cooperative transportation of a load using nonholonomic mobile robots. *Procedia Eng.* 41 (2012), 860–866.
- Nakamura, Y., Ezaki, H., Tan, Y., Chung, W., 2000. Design of steering mechanism and control of nonholonomic trailer systems. In: *Proceedings 2000 ICRA*. San Francisco, CA, USA, 2000, pp. 247–254.
- Ohashi, F., Kaminishi, K., Figueroa Heredia, J.D., et al., 2016. Realization of heavy object transportation by mobile robots using handcarts and outrigger. *Robomech. J.* 3, 27. doi:10.1186/s40648-016-0066-y.
- Svestka, P., Vleugels, J., 1995. Exact motion planning for tractor-trailer robots. In: *Proceedings of 1995 IEEE International Conference on Robotics and Automation*, Nagoya, Japan, 3, pp. 2445–2450.
- Tuci, E., Alkilabi, M., Akanyeti, O., 2018. Cooperative object transport in multi-robot systems: a review of the state-of-the-art. *Frontier in Robotics and AI*.